Microfluidics and Nanofluidics (2022) 26:40
https://doi.org/10.1007/s10404-022-02545-z

RESEARCH PAPER

Analytical model describing the nonlinear behavior of an elastomeric pump membrane in a microfluidic network

Hannah Bott[1] · **Aaron Dörr**[1] · **Jochen Hoffmann**[1] · **Franz Lärmer**[1]

Received: 21 February 2021 / Accepted: 29 December 2021 / Published online: 10 May 2022

Abstract

For several decades, there has been a strong research interest in microfluidic systems and their applications. To bring these systems to market, a high development effort is often necessary for conceptualization and fabrication of such systems as well as the implementation of automated biological analysis processes. In this context, the simulation of microfluidic processes and entire microfluidic networks is becoming increasingly important, as this allows a significant reduction in development efforts, as well as easy adaptation of existing systems to specific requirements. This work presents an analytical model for elastomeric membrane-based micropumps as well as guidelines on how to apply this model to calculate microfluidic networks. The model is derived from the Young–Laplace equation for a non-prestressed elastomeric membrane with a purely nonlinear deflection as a function of applied pressure. The resulting cubic pressure–volume relation is validated by static measurements of the membrane deflection and the transported volume. The model is further used to calculate transient volume flows induced by a membrane micropump in a microfluidic network by adding Hagen Poiseuille's law. Pressure measurements in the pump chamber confirm the basic assumptions of the model and allow definition of its validity scope. This work lays the foundation for designing elastomeric membrane-based micropumps together with microfluidic networks, estimating maximum flow rates in the system and optimizing pumping frequencies for different microfluidic configurations.

Keywords Micropump · Young–Laplace · Elastomer · Network simulation · Lab-on-Chip · Vivalytic

1 Introduction

1.1 Motivation

Over the last 3 decades research work in the field of microfluidics led to a multitude of different technologies and principles to fabricate and actuate micropumps as a central element of microfluidic networks. Among those, the membrane-based micropumps form a group, which can be further categorized based on their actuation principle and the membrane material. While first the focus was on piezoelectrically actuated silicon-based membrane micropumps (van Lintel et al. (1988), Smits (1990), Richter et al. (1998)), today's research is conducted on a variety of materials and actuation principles. Commonly used elastic membrane materials comprise, e.g. parylene (Johnson and Borkholder (2016)), silicone rubber (Meng et al. (2000), Yoon et al. (2001), Sim et al. (2003)) or polydimethylsiloxane (PDMS) (Unger et al. (2000), Berg et al. (2003), Grover et al. (2003), Jeong et al. (2005), Tuantranont et al. (2007), Yang and Liao (2009), Chia et al. (2011), Ni et al. (2012), Mohith et al. (2019)).

Further, compared to silicon or other materials with higher bending stiffness, elastomeric-based micropumps comprise a higher compression ratio, which makes them suitable for self-priming in fluidic operations and enables a larger displacement volume with less energy loss. Among the investigated elastomers, Thermoplastic Polyurethane (TPU) became popular due to its compatibility with organic solvents (Piccin et al. (2007), Wu et al. (2012)), suitability for rapid prototyping (Shaegh et al. (2015), Shaegh et al. (2018), Podbiel et al. (2020)) as well as its biocompatibility and thermo-mechanical properties (Shaegh et al. (2018), Pergal et al. (2013), Pourmand et al. (2018)). An outstanding property of TPU is its softness and, therefore, the purely non-linear behavior of a non-prestressed membrane.

One example for a microfluidic system based on pressure-driven TPU-membrane micropumps is the Lab-on-Chip (LoC) system *Vivalytic* from Bosch Healthcare Solutions

✉ Hannah Bott
hannah_bott@outlook.de

[1] 1 Robert Bosch Corporate Research, Robert-Bosch-Campus 1, 71272 Renningen, Germany

GmbH. Different fluidic pathways of the system can be operated based on valve settings. For the setting of the pumping parameters and implementation of fluidic processes, the dynamic of the pump in relation to different fluidic pathways and viscosities must be known. Modeling and simulation offers the possibility to avoid time-consuming experimental adjustment and optimization of the pumping parameters like frequency and valve switching times. Analytical models can describe the pressure-driven displacement of a pumping membrane. Furthermore, these models enable to solve differential equations for the dynamic behavior of the pump operating in different fluidic network configurations straightforward and analytically.

1.2 State of the art for modeling of microfluidic systems

To model the dynamic behavior of micropumps in microfluidic systems, network modelling based on electric-circuit analogy has been established as a common method (Zengerle and Richter (1994), Oosterbroek et al. (1999), Akers et al. (2006), Choi et al. (2010), Oh et al. (2012), Wu et al. (2014), Schwarz et al. (2016)). This requires an appropriate representation of the micropump, modeling its dynamic behavior in interaction with the system.

In their review, Laser et al. stated that the flow rate generated by membrane displacement pumps depends mainly on (i) the stroke volume (ΔV), (ii) the dead volume (V_0) and (iii) the operating frequency (f_{op}) of the pump, as well as (iv) the valve properties and (v) the fluid properties (Laser and Santiago (2004)). Usually these micropumps are characterized by the resulting overall flow rate for various operation frequencies or actuation pressures. They generate a pulsatile flow rate pattern comprising the same frequency as the actuation. Most publications report that the flow rate is linearly increasing with f_{op} until a critical frequency ($f_{op,crit}$) is reached (Woias (2005), Bardaweel and Bardaweel (2013), Bui et al. (2017), Guevara-Pantoja et al. (2018), Jenke et al. (2018), Banejad et al. (2020)). For an incompressible working fluid, the stroke volume for each pump cycle can be derived with flow rate (Φ) through $\Delta V = \Phi / f_{op}$. However, for a pressure actuated elastomeric membrane-based micropump, the pumping characteristic is directly dependent on the fluidic network since the components in the network determine the fluidic resistance and thus the critical frequency. The characterization of the pump often requires elaborate experimental measurements of the flow rate generated under variation of different influencing parameters. For a LoC system with different fluidic pathways, which can be operated based on the valve setting, this characterization becomes even more complex, as the measurement has to be repeated for every possible fluidic configuration. Further, this way of pump characterization does not provide information about the actual time course of the flow rate, which includes maximum values and the duration of a pump cycle. However, these are critical parameters for implementation of fluidic processes in the LoC, as the impact of flow rate induced shear rates can compromise the handling of biological fluids in a microfluidic system. Especially if the physical and biological properties of a sample are sensitive to mechanical forces or shear stresses, resulting shear rates should be considered to transport different analytes in a LoC system (Brooks (1984), Dinhof (2001), Cheung et al. (2011), Salmanzadeh et al. (2012), Au et al. (2017)). Hence, there is a need to model and simulate the dynamic behavior of a micropump in a fluidic network.

For pneumatically actuated, elastomeric membrane-based micropumps, non-linear restoring forces have to be taken into account to model the dynamic response of the membrane. It was already shown that the geometrical displacement of elastomeric membranes follows spherical deformation (Yoon et al. (2010), Wu et al. (2014), Mazloum and Shamsi (2020), Sprague et al. (2020)). However, these studies mainly focus on calculation of the maximum membrane displacement and, therefore, stroke volume of the micropump for different system parameters.

1.3 Aim of this work

Several publications reported the design and fabrication of a TPU-membrane-based micropump (Rupp et al. (2012), Pourmand et al. (2018), Podbiel et al. (2020)). So far, none of the cited work has reported an analytical model and simulation for the pressure-driven displacement of TPU-membrane-based micropumps. The aim of this work is to provide an analytical model for the pneumatically actuated displacement of a TPU-membrane-based micropump featuring a purely non-linear behavior. The intended application of this model is to integrate it into a network modeling program in which individual fluidic components can be arbitrarily interconnected and fluidic processes can be calculated. Therefore, our approach aims to provide a relatively simple and analytical model for the pneumatically actuated displacement of the TPU-membrane-based micropump.

The model will be derived from the Young–Laplace equation, leading to a cubic pressure–displacement law. The derived relation will be verified through measurement of the pressure vs. displacement curve of a securely-clamped, non-prestressed TPU-membrane. The model will enable to solve the differential equations describing the fluidic network based on Hagen–Poiseuille's law. In particular, two different cases are considered: (I) the pump is connected to a prefilled fluidic channel, resulting in a constant fluidic resistance and (II) the pump is connected to a previously empty fluidic channel, resulting in a dynamic fluidic resistance. The model-derived volumes of a pump cycle will be compared to experimentally obtained volumes for different actuation pressure levels. The dynamics of the model is verified by transient pressure measurements inside the pump chamber. Furthermore, the model will be expanded to include different actuation courses as pressure functions, to be able to calculate the effect of system dependent variances. The effect of different actuation courses on the dynamic membrane behavior will be implemented in the model by a convolution with the pressure function. Parameter simulation studies will be done to estimate maximum occurring flow rates and pump cycle durations depending on the fluidic resistance for different system configurations.

2 Concept and modeling

In this section, we set up an analytical model describing the non-linear pressure-driven displacement behavior of a non-prestressed elastomeric-membrane-based micropump. For example, this model is applicable to the micropump, which is integrated in the LoC system *Vivalytic*. A schematic cross-section of such a pump unit is displayed in Fig. 1. The membrane is displaced through the actuation pressure $p_{\text{actuation}}$. Hence, the membrane can be pulled, to open and fill the pump chamber or pushed to close and empty the pump chamber. As it is a common simulation practice, we first build the model with an analytical derivation of the membrane behavior based on different

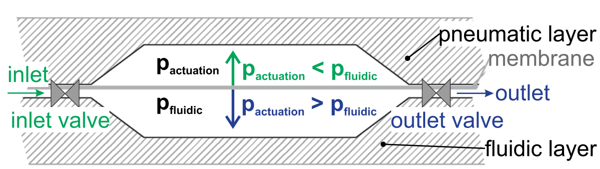

Fig. 1 Schematic cross-section and operating principle of a membrane based, pressure-driven pump unit with inlet and outlet valves. The valves are only shown as symbols. The functional unit is formed of a three-layer stack, containing a pneumatic layer and a fluidic layer, which are, for example made of microstructured polycarbonate. Both layers contain channels for the pneumatic control of the chambers and valves in the LoC system (not shown here). The layers are separated by an elastomeric membrane, for example TPU. Different valves can be chosen according to the transport path that is required for the fluidic process. © IOP Publishing. Reproduced with permission from Bott et al. (2021). All rights reserved

assumptions and simplifications. To specify the model parameters we use literature values and experimentally determined parameters. Then we set up and solve a differential equation based on Hagen–Poiseuille's law describing the dynamic of the pump in a microfluidic network. The model and the analytical solution for the differential equation are implemented in Matlab to run the simulation experiments. The dynamic behavior of the micropump in the fluidic network is then determined with regard to the influence of the fluidic resistance as well as the dependence on the actuation force and time control of the pump.

2.1 Model assumptions and approximations

To set up the model for the pressure-driven, elastomeric-membrane-based micropump it is connected to a fluidic network with the fluidic or hydrodynamic resistance (R_h).

The pump unit requires two valves as inlet and outlet to direct the fluid flow in the system. The valve selection varies depending on the fluidic process (as described in Podbiel et al. (2020)). The valves are actuated through independent pneumatic ports. A flat valve seat ensures that the valve is completely closed when positively pressurized and admits fluid flow under negative pressure. The influence of the valves on the fluidic resistance is assumed to be small compared to the channels in the system. Hence, in the model the valves of this pump unit are assumed to be ideal ($p_{\text{forward}} = 0$ and $p_{\text{reverse}} \rightarrow \infty$, see Laser and Santiago (2004)).

Furthermore, the TPU-membrane is assumed to be non-prestressed with negligible inherent rigidity and fixed at its borders, which corresponds to its mounting condition in the LoC system *Vivalytic*. As the maximum displacement of the membrane is small compared to its lateral dimensions, a constant E-modulus is assumed in the considered dynamic range as well as incompressibility of the TPU.

One challenge posed by the use of elastomeric membranes for micropumps are volume variations resulting from pressure variations in the system and the possibility of overstressing the membrane. To overcome this, the membrane displacement can be limited through stoppers in the pump chamber in both directions of deflection (as shown in Fig. 1). The modeling of a limit stop at membrane deflection can have a high complexity depending on the structure of the membrane and the contact area (Henning (2003), Henning (2006)). To avoid increased complexity of the model, the limit stop is implemented through cutting off the pumping operation at a definite point, or rather the maximum volume of the pump chamber and the minimal volume, respectively. The admissibility of this assumption will be investigated by the experimental results and discussed in Sects. 4.2 and 4.3. The validity of this simplification was further investigated by numerical simulation as illustrated in the Appendix (Figs. 9, 11, 12). It showed that the residual volume in the pump chamber after first contact of the membrane with the chamber limit stop is about 3.88 µL, corresponding to about 13 % of the whole pump chamber volume.

2.2 Cubic pressure–volume law

As this study is looking at the transient change of the volume inside the pump chamber or the volume that is pumped into or out of the pump chamber, respectively, the focus is on $V = V(t)$ or rather $t = t(V)$.

As a first step, the relation between the applied pressure and the membrane displacement, or rather the displaced volume is derived from the Young–Laplace equation (Young (1805), Laplace (1805)). If the Young–Laplace equation is used to determine the two angles of a curved interface, or rather the shape of a membrane that is displaced by an external pressure, it results in

$$\Delta p = \frac{2 \cdot \sigma \cdot d}{R}, \tag{1}$$

where σ is the isotropic stress in the membrane, d is the thickness of the membrane, R is the radius of curvature and Δp is the pressure operating on the membrane. For a spherical elongation of the membrane, the shape of the membrane can be described in a 2-dimensional case as a circle segment with R being the radius of curvature and l' the membrane diameter for a certain elongation position of the membrane (see Fig. 2).

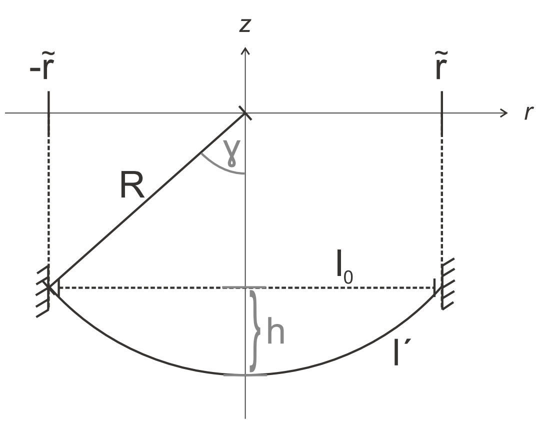

Fig. 2 Geometrical, 2-dimensional representation for the displacement of a circular membrane with radius $\tilde{r}$ derived from the Young–Laplace equation. l_0 indicates the membrane diameter for its non-elongated equilibrium position. l' indicates the membrane diameter for an elongated position of the membrane with angle γ and curvature R at the displacement distance h of the membrane center from its equilibrium

As the maximum displacement is small compared to the lateral dimensions of the membrane, a small longitudinal elongation can be assumed and the membrane operates within its elastic limit. This leads to the assumption that the elongation of the membrane is constant for a certain pressure. Then, the elongation of the membrane for an applied pressure p follows from Hooke's law for elastic materials, which is

$$\sigma = \frac{1}{(1-\nu)} \cdot \epsilon \cdot E. \tag{2}$$

generalized for isotropic materials subjected to a normal force in one direction (see Young and Budynas (2002)). Here, E is the elastic modulus of the membrane, ϵ is the strain tensor and ν the Poisson's ratio. For a constant E, ϵ is obtained from

$$\epsilon = \frac{\Delta l}{l_0} = \frac{l' - l_0}{l_0} \tag{3}$$

with l_0 being the diameter of the non-elongated membrane and l' being the diameter of the elongated membrane. For the elongated membrane as a spherical segment with the curvature radius R and with $\tilde{r}$ being the radius of the circular, non-elongated membrane, the diameter l' results in (Bronstein and Semendjajew (1991), p.194)

$$l' = 2 \cdot R \cdot \gamma = 2 \cdot R \cdot \arcsin\left(\frac{\tilde{r}}{R}\right). \tag{4}$$

With a power series expansion for $\arcsin(x)$ (Bronstein and Semendjajew (1991), p.33), eq. (4) becomes

$$l' = 2 \cdot \tilde{r} + \frac{1}{3} \cdot \frac{\tilde{r}^3}{R^2} + \frac{3}{20} \cdot \frac{\tilde{r}^5}{R^4} + \mathcal{O}(\tilde{r}^7) \tag{5}$$

and thereof with $l_0 = 2 \cdot \tilde{r}$, eq. (3) results in

$$\epsilon = \frac{l' - 2 \cdot \tilde{r}}{2 \cdot \tilde{r}} = \frac{1}{6} \cdot \frac{\tilde{r}^2}{R^2} + \frac{3}{40} \cdot \frac{\tilde{r}^4}{R^4} + \mathcal{O}(\tilde{r}^6). \tag{6}$$

With h as the displacement position of the membrane center from the zero line the radius of curvature can be written as (Bronstein and Semendjajew (1991), p.200)

$$R = \frac{\tilde{r}^2 + h^2}{2h}. \tag{7}$$

Now, eqs. (2), (6) and (7) inserted into the Young–Laplace eq. (1) result in

$$\Delta p = \frac{8}{3} \cdot \frac{E \cdot d}{(1-\nu)} \cdot \frac{h^3}{\tilde{r}^4} + \mathcal{O}(h^5). \tag{8}$$

With a Poisson's ratio of $\nu = 0.5$ for TPU (derived from Tsukinovsky et al. (1997)) equation (8) becomes

$$\Delta p \approx \frac{16}{3} \cdot \frac{E \cdot d}{\tilde{r}^4} \cdot h^3 \tag{9}$$

showing that for small h the membrane follows a cubic pressure -displacement law. Here, E is the parameter reflecting the membrane elastic properties and can be obtained experimentally from the pressure–displacement behavior of the membrane, as shown in Sect. 2.3.

As it was demonstrated, for a pressure-driven micropump with a fixed, non-prestressed TPU-membrane a cubic relation for the displacement distance h as a function of the pressure Δp can be assumed. To relate the applied pressure to the displaced volume, the equation

$$V = \frac{3 \cdot \tilde{r}^2 \cdot \pi \cdot h}{6} + \frac{\pi \cdot h^3}{6} \approx \frac{3 \cdot \tilde{r}^2 \cdot \pi \cdot h}{6} + \mathcal{O}(h^3) \tag{10}$$

is valid for a circular membrane with the radius $\tilde{r}$ (Bronstein and Semendjajew (1991), p.200). From eq. (10) follows

$$h = \frac{2 \cdot V}{\pi \cdot \tilde{r}^2} \tag{11}$$

for small displacement distances h with V as the volume that is displaced by the membrane, which leads to a cubic pressure–volume law:

$$\Delta p = \frac{128}{3} \cdot \frac{E \cdot d}{\tilde{r}^{10} \cdot \pi^3} \cdot V^3 \tag{12}$$

Introducing a constant parameter

$$c = \frac{128}{3} \cdot \frac{E_{\text{membrane}} \cdot d_{\text{membrane}}}{r_{\text{pump}}^{10} \cdot \pi^3} \tag{13}$$

for the membrane-based micropump with fixed constraints at radius $\tilde{r} = r_{\text{pump}}$, elastic modulus E_{membrane} and thickness d_{membrane}, now leads to the cubic pressure-volume law

$$p = p(V) = p_0 - c \cdot V^3 \tag{14}$$

which is applicable for a membrane-based, pressure actuated micropump with a non-prestressed membrane with fixed constraints.

2.3 Model parameters

The constant parameter c (see eq. (13)) is the characteristic parameter for the pump model. It is dependent on the geometry of the pumping membrane, including the membrane thickness d_{membrane} and the lateral dimensions of the fixed membrane (e.g. r_{pump} = the radius of a circular membrane).

The shape of the pumping membrane of the investigated micropump is closer to an elliptic than to a circular shape. Here, the ellipticity factor ϵ_E correlates the two main axes r_1 and r_2 through

$$r_2 = r_1 \cdot (1 + \epsilon_E). \tag{15}$$

With eq. (15) the model derivation from the Young–Laplace eq. (1) can be carried out simultaneously, starting from the modified Young–Laplace equation

$$\Delta p = \frac{\sigma \cdot d}{R_1} \cdot \left(1 + \frac{1}{1 + \epsilon_E}\right). \tag{16}$$

To estimate c, a substitute radius r_s is used for the membrane radius r_{pump} which is derived from the two radii by

$$r_s = \sqrt{r_1 \cdot r_2}. \tag{17}$$

For the here investigated pump chamber with the two main axes radii $r_1 = 2.815$ mm and $r_2 = 4.115$ mm the corresponding substitute radius is $r_{s1} = 3.403$ mm.

Furthermore, the constant parameter c is dependent on the elastic modulus of the membrane which was obtained experimentally according to Sect. 3.1.

2.4 Volume flow rate

In this section, the volume flow rate is derived by solving the differential equation for a micropump connected to a hydrodynamic network. The volume flow Φ (as V, the time derivation of V) out of the pump with a connected hydrodynamic resistance R_h is

$$\Phi = \frac{\Delta p}{R_h} \tag{18}$$

which is based on Hagen–Poiseuille's law. From this follows the differential equation

$$\Phi = \dot{V} = \frac{p_0}{R_h} - \frac{c}{R_h} \cdot V^3. \tag{19}$$

Here, p_0 is the actuation pressure for the membrane pump which is either positive (e.g. + 1.5 bar over atmospheric pressure) to eject the volume out of the pump chamber or negative (e.g. − 0.8 bar) to suck the volume into the pump chamber. Volume flow happens as long as the driving pressure $p = p_0 - c \cdot V^3$ is > 0, so the equilibrium state for the displaced membrane is reached, when

$$p_0 - c \cdot V_0^3 = 0 \tag{20}$$

which leads to

$$V_0 = \sqrt[3]{\frac{p_0}{c}} \tag{21}$$

The solution of the differential eq. (19) is the following equation (see Bronstein and Semendjajew (1991), p.39):

$$t(V_{\text{norm}}) = \frac{R_h}{c \cdot V_0^2} \cdot \left[\frac{1}{6} \cdot \ln\left(\frac{1 + V_{\text{norm}} + V_{\text{norm}}^2}{\left(1 - V_{\text{norm}}\right)^2}\right) + \frac{1}{\sqrt{3}} \cdot \left[\arctan\left(\frac{2 \cdot V_{\text{norm}} + 1}{\sqrt{3}}\right) - 0.52\right]\right] \tag{22}$$

with

$$V_{\text{norm}} = \frac{V}{V_0} = [0, 1]$$

$$\arctan(\frac{1}{\sqrt{3}}) \approx -0,52$$

and with

c implying the membrane parameters
R_h implying the hydrodynamic resistance of the fluidic network.

To describe a whole suction or ejection process of the micropump by the membrane deflection, two phases have to be considered in each case. The suction and ejection process of the membrane and the forces acting on the membrane during the deflection are illustrated in Fig. 3.

In case of the *ejection* process, the actuation pressure is switched from negative pressure ($P_{vac} = -0.8$ bar) to positive pressure ($P_{op} = 1.5$ bar). As long as the membrane is deflected above its neutral position, the elastic restoring force of the membrane contributes to the ejection process in addition to P_{op}. In this case, to compute $t(V)$ with eq. (22), starting from a deflected membrane by the negative pressure, is reflected through negative values for the volume from $-V_{max}$ to 0 until the membrane reaches its neutral position. For the continued ejection process, the elastic restoring force of the membrane increases as the membrane is deflected until its maximum displacement position. Now this force acts in the opposite direction of the actuation pressure and, therefore, reduces the net force deflecting the membrane. In this case, to compute $t(V)$ with eq. (22), positive values for the volume from 0 to V_{max} are taken to reflect the ejection process from the neutral position of the membrane to its maximum deflection. Altogether, the ejection process is now reflected through the integration of the volume in the pump chamber from the negative volume $-V_{\text{max}}$ (which in the following is referred to as the volume for applied vacuum V_{vac}) to the positive volume $+V_{\text{max}}$ (which in the following is referred to as the volume for applied vacuum V_{op}). The pumped volume at every time step can be calculated as

$$\Delta V(t) = V(t) - V_{vac}. \tag{23}$$

The corresponding equations apply for the *suction* process: here, the actuation pressure is switched from positive pressure ($P_{op} = 1.5$ bar) to negative pressure ($P_{vac} = -0.8$ bar). As long as the membrane is deflected below its neutral position, the elastic restoring force of the membrane contributes to the suction process in addition to P_{vac}. In this case, to compute $t(V)$ with eq. (22), starting from a deflected membrane by the positive pressure, is reflected through positive values for the volume from V_{max} to 0 until the membrane

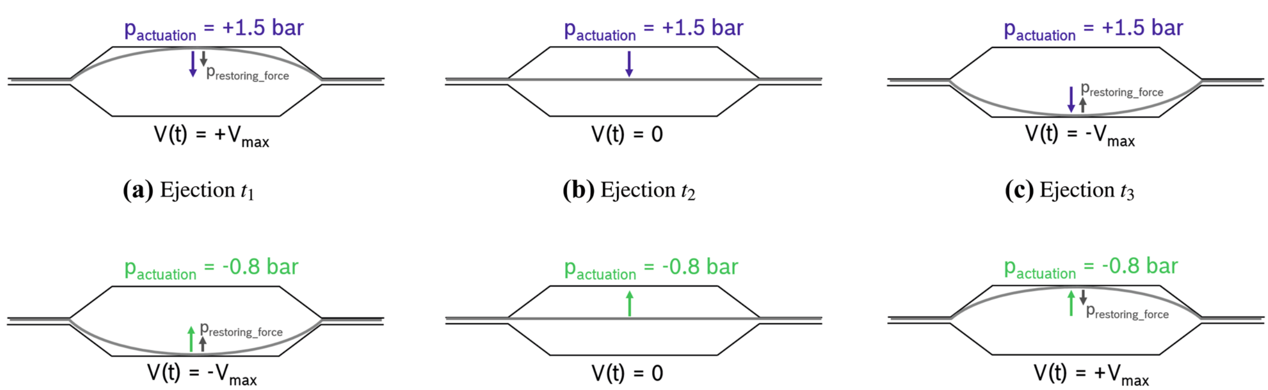

(a) Ejection t_1 **(b)** Ejection t_2 **(c)** Ejection t_3

(d) Suction t_1 **(e)** Suction t_2 **(f)** Suction t_3

Fig. 3 Ejection and suction process of a TPU-membrane-based pump chamber with non-linear pressure–displacement behavior. The arrows indicate the forces acting upon the membrane for the membrane positions at t_1—phase 1, t_2—transition phase and t_3—phase 2. If the membrane is displaced until the limit stop of the pump chamber, the restoring force (grey) is maximal. At the equilibrium position of the membrane (**b**) and **e** the membrane is in a non-prestressed condition and no additional restoring forces are acting in addition to the actuation force reaches its neutral position. For the continued suction process, the elastic restoring force of the membrane increases while the membrane is deflected until its maximum displacement position. Now this force acts in the opposite direction of the actuation pressure and, therefore, reduces the net force acting on the membrane. In this case, to compute $t(V)$ with eq. (22), negative values for the volume from 0 to $-V_{\max}$ are taken to reflect the suction process from the neutral position of the membrane to its maximum deflection. Altogether, the suction process is now reflected through the integration of the volume in the pump chamber from the positive volume $+V_{\max}$ (V_{op}) to the negative volume $-V_{\max}$ (V_{vac}). The pumped volume at every time step can be calculated as

$$\Delta V(t) = V(t) - V_{op}. \tag{24}$$

The equation for $t(V)$ now describes the pump characteristic as a function of a hydraulic resistance R_h that is connected to the pump. Because of the complex formula, the equation cannot be inverted analytically to obtain a coherent expression for $V(t)$. However, it can be inverted numerically, e.g. by computing the values of t for different V, or graphically, as the $t(V)$ diagram with the pump characteristic curve can be inverted by just switching the axis for t and V. An example for qualitative pump characteristic curve for $t(V)$ as well as $V(t)$ with arbitrarily selected values for c and R is shown in Fig. 4.

Furthermore, the resulting flow rate can be obtained by the temporal derivation of $V(t)$ which leads to the volume flow rate profile as a function of time:

$$\Phi(t) = \dot{V}(t). \tag{25}$$

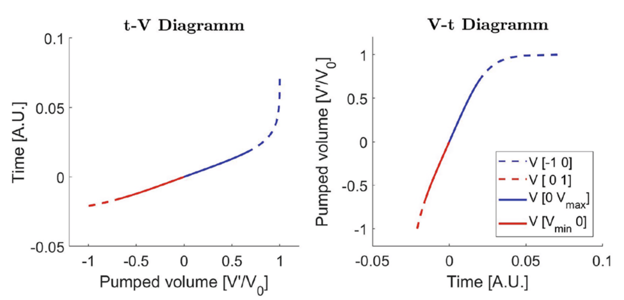

(a) $t(V)$ **(b)** $V(t)$

Fig. 4 Example of (**a**) a qualitative pump characteristic curve $V(t)$ (according to eqs. (23) and (24)) and **b** its time derivative $\Phi(t)$ (according to eq. (25)) for a pressure-actuated, TPU-membrane-based micropump with non-linear behavior. Values for c and R are selected arbitrarily, so the curve is displayed with arbitrary time units. The dashed line describes $V(t)$ and $\Phi(t)$ if the membrane is displaced without a limit stop, the solid line shows $V(t)$ and $\Phi(t)$ if the membrane is displaced against a limit stop with a maximum pump chamber volume $V_{\max} < V_0$

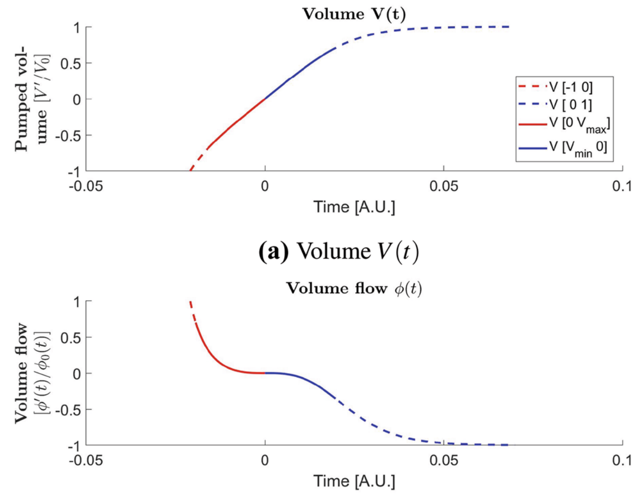

(a) Volume $V(t)$

(b) Volume flow $\Phi(t)$

Fig. 5 Example of (**a**) a qualitative pump characteristic curve describes $V(t)$ (according to Eqs. (23) and (24)) and (**b**) its time derivative $\Phi(t)$ (according to Eq. (25)) for a pressure-actuated, TPU-membrane based micropump with non-linear behavior. Values for c and R are selected arbitrarily, so the curve is displayed with arbitrary time units. The dashed line describes $V(t)$ and $\Phi(t)$ if the membrane is displaced without a limit stop, the solid line shows $V(t)$ and $\Phi(t)$ if the membrane is displaced against a limit stop with a maximum pump chamber volume $V_{\max} < V_0$

An example for qualitative pump characteristic curve for $V(t)$ as well as its derivative $\Phi(t)$ with arbitrarily selected values for c and R is shown in Fig. 5.

The constant parameter c results from the experimentally determined membrane parameter E_{membrane} as shown in Sect. 2.3. To calculate R in the fluidic network, two cases are now to be considered:

(I) Pumping through a prefilled channel of finite length.
(II) Pumping through a previously empty channel of infinite length.

For case (I) the hydraulic resistance R_h can be assumed as constant for the flow of an incompressible, Newtonian fluid with viscosity η though a microfluidic channel. Assuming laminar flow conditions it follows from the Poiseuille equation (Poiseuille (1846)) that

$$R_{h\_static} = \frac{\Delta p}{\Phi} = \frac{2 \cdot \eta \cdot L \cdot P^2}{A^3} \tag{26}$$

with L being the length, P the perimeter and A the area of an arbitrarily shaped channel in the microfluidic network. For a circular channel with radius r_{channel} it follows

$$R_{h\_static} = \frac{8 \cdot \eta \cdot L \cdot \pi}{A^2} \tag{27}$$

with

$$A = 2 \cdot \pi \cdot r_{\text{channel}}^2 \tag{28}$$

For case (II) the hydraulic resistance changes dynamically as the part of the channel that is filled with fluid increases during the pumping process. In this case R_h is a function of time, or rather a function of the current length of the channel that is filled with fluid. This length is a function of the Volume $V(t)$ that is already pumped at a certain time and the cross section area A of the channel:

$$L(t) = \frac{V(t)}{A} \tag{29}$$

Inserted in eq. (27) this leads to

$$R_{h\_dyn}(t) = \frac{8 \cdot \eta \cdot \pi}{A^3} \cdot V(t) \tag{30}$$

for a dynamically increasing resistance during the pumping process into a previously empty channel. Equation (19) can be written as

$$\dot{V} = \frac{c}{R_h} \cdot \left(\frac{p_0}{c} - V^3 \right) = \frac{c}{R_h} \cdot \left(V_0^3 - V^3 \right) \tag{31}$$

which leads to the differential equation

$$\dot{V} = \frac{c \cdot A^3}{8 \cdot \pi \cdot \eta \cdot V} \cdot \left(V_0^3 - V^3 \right). \tag{32}$$

Equation (32) can be written as

$$\frac{V \cdot \dot{V}}{V_0^3 - V^3} = \frac{c \cdot A^3}{8 \cdot \pi \cdot \eta} \tag{33}$$

Integration and solving the differential equation (Bronstein and Semendjajew 1991, p.39) leads to the analytical solution

$$\begin{aligned} t(V, R_{h\_dyn}) = & \frac{8 \cdot \pi \cdot \eta}{c \cdot A^3 \cdot V_0} \cdot \left[\frac{1}{6} \cdot \ln \left(\frac{1 + V_{\text{norm}} + V_{\text{norm}}^2}{\left(1 - V_{\text{norm}}\right)^2} \right) \right. \\ & \left. + \frac{1}{\sqrt{3}} \cdot \left[\arctan \left(\frac{2 \cdot V_{\text{norm}} + 1}{\sqrt{3}} \right) - 0.52 \right] \right]. \end{aligned} \tag{34}$$

Again, $V(t)$ can be found numerically or graphically by 'inverting' $t(V)$. The derived equations now allow to calculate any configuration for a microfluidic network consisting of the modeled TPU-membrane-based micropump and microfluidic channels. The hydrodynamic resistance of the channel is either static if the channel of a finite length L is prefilled with fluid (see eq. (26)) or changes dynamically with the filling level if the channel of infinite length is not prefilled with fluid (see eq. (30)). For a combination of prefilled and not prefilled channels the static and dynamic resistances can be added, which results in:

$$R_{h\_static,dyn}(t) = R_{h\_static} + R_{h\_dynamic}(t) \tag{35}$$

3 Experimental methods

3.1 E-Modulus

The constant parameter c is dependent on the elastic modulus of the membrane (see eq. (13)) which was obtained experimentally by a standardized tensile test for a testing speed of 1 mm/min.To verify the model assumptions leading to the cubic pressure–displacement law in eq. (9), the E-modulus was also determined by measuring the relation between the displacement of a fixed, non-prestressed TPU-membrane with circular boundaries and the pressure that is applied on the membrane. Different pressure levels were applied through an electronic pressure regulator (type: PCD-15PSIG-D/5P 5IN, Natec Sensors GmbH). Displacement was measured optically with a microscope (type: BX 61, Olympus Europa SE & Co. KG) by determining the position of the focus plane on the membrane surface. The data were then fitted to the cubic pressure - displacement law.

3.2 Pressure measurement

The derived model was verified through pressure measurements in the pump chamber of the LoC system *Vivalytic*. The pressure sensor (LabSmith-uPS0250-T116-10, Mengel Engineering, Virum, Denmark) was adapted directly to the pump chamber ensuring minimal capacity-related delays. To ensure a sufficient temporal resolution of the pressure measurement and allow to neglect the system capacities, a high viscosity fluid (Silicone oil, 100cSt) was used. The resulting high fluidic resistance entailed a duration of the ejection process in the range of a few seconds.

3.3 Parameter study

A parameter study was done with the derived analytical model to deduce maximum flow rates and pump cycle durations for generic system configurations. The model setup and example curves from Sect. 2.4 were done with arbitrary values for the fluidic parameters. Now the model was applied to the here investigated microfluidic system, to determine and predict the characteristic curves of the membrane-based, pressure-driven micropump of the LoC system *Vivalytic*.

To determine the influence of various fluidic parameters like channel length and fluid viscosity the maximum flow rates were taken into account as well as the duration for emptying a pump chamber completely. System-related values were fixed for the parameter study. These include the E-modulus of the TPU-membrane, which was determined in Sect. 2.3, the pressure level ($p_0 = 1.2$ bar) that is applied as the actuation force for the micropump, and the hydraulic radius ($r_{\text{channel}} = 234\mu m$) which is the same for all channels of the microfluidic network. Variable parameters are, therefore, (i) the length of the microfluidic channel, which is determined through the setting of the valves of the microfluidic network, as well as (ii) the viscosity of the fluid to be transported through the microfluidic system.

4 Results and discussion

4.1 E-Modulus

The elastic modulus of the membrane was obtained experimentally by a standardized tensile test. The resulting E-modulus for a testing speed of 1 mm/min was $E_{\text{membrane}} \approx 33.5$ MPa.

The measurement results for the relation between the displacement of the TPU-membrane with circular boundaries and the pressure that is applied on the membrane are shown in Fig. 6, verifying the cubic pressure–displacement behavior of the TPU-membrane. The measurement result implies an elastic modulus of $E_{\text{membrane}} \approx 35.6$ MPa which is comparable with the measurement result of the standardized tensile test.

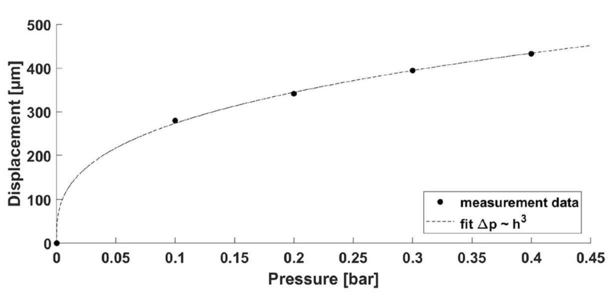

Fig. 6 Measurement points for the pressure dependent displacement of a TPU-membrane with circular constraints ($r = 2500\mu m$). Different pressure levels were applied through an electronic pressure regulator (type: PCD-15PSIG-D/5P 5IN, Natec Sensors GmbH). Displacement was measured optically with a microscope (type: BX 61, Olympus Europa SE & Co. KG) by determining the position of the focus plane on the membrane surface. The data can be fitted to the cubic pressure–displacement law in (eq. (9)). The mean value of the resulting E-modulus of the TPU-membrane for the obtained measurement points is $E_{\text{membrane}} \approx 35.6$ MPa

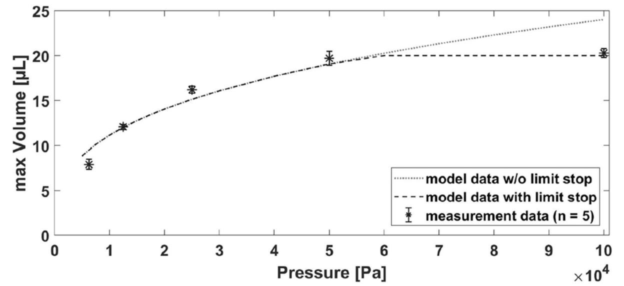

Fig. 7 Measurement and model data for the pressure to volume displacement ratio of the TPU-membrane-based, pressure-driven micropump of the LoC system *Vivalytic*. For the measurement of average pumped volume per cycle the mean of 50 pump cycles was taken and this measurement was repeated 5 times. The parameters for the model calculation were $E_{\text{membrane}} \approx 35.6$ MPa (see Sect. 2.3) and $r_{\text{pump}} = 3.8$ mm (substitute radius for the used pump chamber)

4.2 Static measurements

The displaced volume predicted by the presented model for one pump cycle was compared with experimentally obtained data from the LoC System *Vivalytic*. The result for different pressure levels is displayed in Fig. 7. The measurement data show a good agreement with the volume prediction by the model. The graph also shows the comparison between the model with limit stop and without limit stop. Modeling the limit stop by cutting off the volume at the maximum seems to be a good approximation for determining the volume per pump cycle.

4.3 Transient measurements

The pressure course in the pump chamber was measured according to Sect. 3.2 and the result is displayed in Fig. 8. Integrating the curve of the measured pressure difference allowed to obtain the pumped volume over time and to extract the two phases of the ejecting process: phase 1, where the membrane is moving towards the equilibrium position (see Fig. 3a) and phase 2, where the membrane is moving away from the equilibrium position (see Fig. 3c). The membrane is in equilibrium position, when half of the volume is ejected from the pump chamber (dashed line at $V = 12.5\mu L$). The derived time of the equilibrium position ($\Delta t \approx 1$s) corresponds to the inflection point of the measured pressure curve. The measurement shows a quite good qualitative agreement with the model derived volume over time, which confirms the general approach and the assumptions of the presented model. In the second phase of the pump cycle, model and measurement start to diverge which is probably mainly due to modeling the limit stop by just cutting off the curve at a maximum pump chamber volume of 25 μL. This could be tackled by introducing a counter force into the model, which reflects the increasing resistance when the membrane is pressed against the pump chamber limit stop.

4.4 Parameter study

A parameter study was done according to Sect. 3.3. The E-modulus $E_{membrane} \approx 35.6$ MPa resulting from Sect. 4.1 was used for the study. The results of the parameter study are shown in Table 1. The maximum flow rate and the duration of one pump cycle are taken from the flow rate profile for each parameter setting. All parameters were set and investigated in the range they occur in microfluidic processes on the LoC system *Vivalytic*. Fluid viscosities of 1cSt and 10cSt were investigated to cover the range of fluid viscosities mainly used in the system. Maximum flow rates vary from 1273 $\frac{\mu L}{s}$ for a channel length of 100 mm and a fluid viscosity of 1 cSt to 64 $\frac{\mu L}{s}$ for a channel length of 200 mm and a fluid viscosity of 10 cSt. The duration for one pump cycle varies between 27 ms and 541 ms, respectively.

4.5 Enhanced model with transient actuation parameter

To map the model with the actual operating conditions of the LoC system *Vivalytic*, the profile of the actuation pressure needs to be considered in the model. So far, the actuation pressure was set as a constant, instantaneously applied pressure that is acting on the pumping membrane. However, for the real system the delay time of switching between vacuum and overpressure or vice versa needs to be considered as well, to involve the time needed to build up the pressure at the pumping membrane. The actuation pressure profile of a test bench for the LoC system was determined by a pressure sensor (BMP388, Bosch Sensortec GmbH, Reutlingen, Germany). The result of the pressure measurement is shown in Fig. 9. It demonstrates that the time delay for switching between applied vacuum and overpressure takes up to 50 ms and the time to build up the pressure at the pumping membrane takes up to 75 ms. This result confirms the hypothesis that the profile of the actuation pressure needs to be considered in the model description of the system as one pump cycle proceeds in the same time range.

To implement the actuation parameter p_0 as a time-dependent function, in the model, the measured pressure profile was convoluted with the analytical solutions of eq. (32). The resulting volume over time and derived volume flow rate over time for a channel length of 200 mm is displayed in Fig. 9 for both: the assumption of an instantaneous pressure jump (dotted line) and for the measured pressure course (solid line). The comparison shows that a delayed build-up of pressure increases the pump cycle duration but reduces the maximum occurring flow rates.

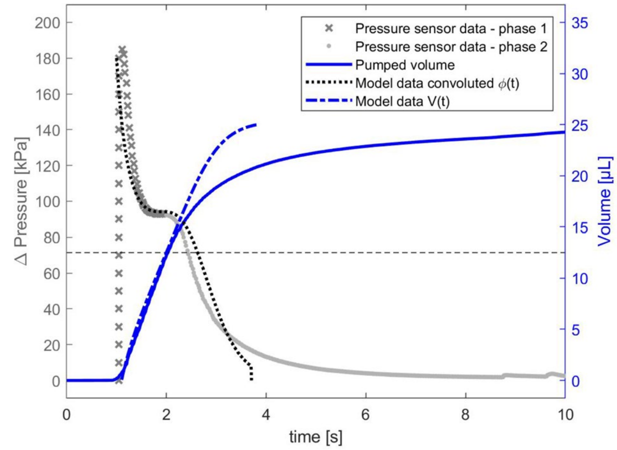

Fig. 8 Measurement and model data for the transient volume displacement of the TPU-membrane-based, pressure-driven micropump of the LoC system *Vivalytic*. For the measurement, the pressure sensor was adapted directly to the pump chamber. The pressure course was measured during a pump cycle while pumping a high viscosity silicone oil (100 cSt) through a channel with length a of 200 mm. The parameters for the model calculation were taken from Sect. 2.3 with a pressure level of $p_0 = 1.2$bar. The dashed line at $V = 12.5\mu L$ shows the equilibrium position of the membrane, when half of the volume is ejected from the pump chamber. Model and measurement data show a good agreement for phase 1 of the pump cycle and start deviating in phase 2 (see Fig. 3)

Table 1 Results of the parameter study with the analytical model. Maximum flow rates and pump cycle durations are obtained for variable channel lengths l and viscosities ν

Model parameter	Maximum flow rate [$\mu L/s$]	Pump cycle duration [ms]
ν = 1 cSt		
l = 100	1273	27
l = 150	849	41
l = 200	637	54
l = 200 mm		
(ν) = 5	127	270
(ν) = 10	64	541

4.6 Discussion

The step-by-step guidelines for an analytical model that describes the non-linear deflection of an elastomeric membrane, and calculates dynamic fluid processing, are a powerful tool for developing pressure-driven microfluidic systems. Maximum flow rates occurring in microfluidic systems are a critical factor, for example for sequential filling of compartments where emulsions and air bubble entrapment must be avoided, or when handling biological sample materials like

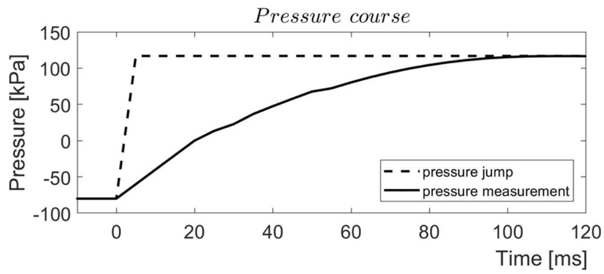

(a) Pressure course $p(t)$

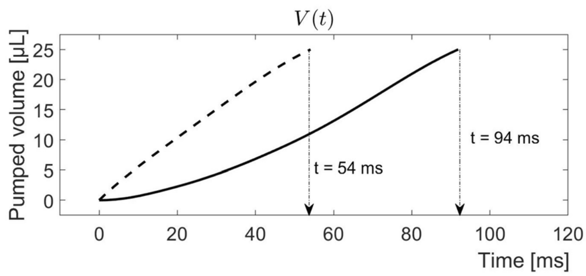

(b) Volume $V(t)$

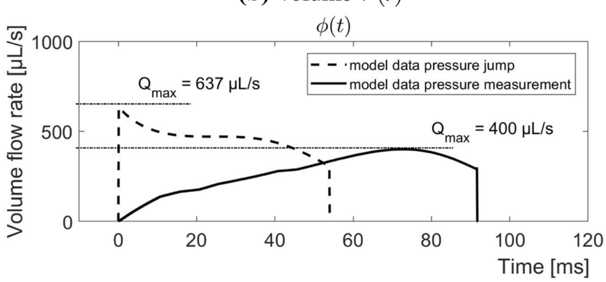

(c) Convoluted volume flow $\Phi(t)$

Fig. 9 Convolution of $V(t)$ and the measured pressure profile for the actuation pressure of a research test bench to process the LoC system *Vivalytic*. **a** The measured pressure profile shows that the ramping time-constant from the applied vacuum of − 80 kPa to 0 kPa is about 25 ms and ramping up to the maximum overpressure of 120 kPa takes about 75 ms. The graphs display (**b**) the pumped volume over time and **c** the derived volume flow rate over time as a result of the convolution of the pressure function with the analytical model for $t(V)$ (see eqs. (23)–(25))

cells which are sensitive to shear stresses. For setting and optimizing pumping frequencies for different fluidic parameters and system configurations, it is also relevant to know the duration of a pump cycle.

For a pump chamber where the deflection of the diaphragm is restrained by a limit stop, the assumption was made that the process in the model can be cut off when the maximum volume is reached. However, this assumption neglects additional forces that affect the membrane displacement when the membrane is displaced against the solid boundary of the pump chamber like in the actual setting. The results of the dynamic pressure measurements suggest that this assumption may lead to a deviation from the model with the actual course of the volume flow in the second phase of the pumping process (see Fig. 8). One way to address this deviation would be to include the limit into the model as a counterforce that builds up depending on the application of the diaphragm to the pump chamber.

The computation of the hydraulic resistance in the model through the Poiseuille equation (eq. (26)) is based on the assumption of laminar flow conditions. Flow rates $> 1000\frac{\mu L}{s}$ may result in a Reynolds number > 2200 even in microfluidic channels. This is the range of transition from laminar to turbulent flow profiles in microfluidic systems (Nguyen and Wereley (2006)). Consequently, for our investigated system the model assumptions work well to determine the flow rate profile within an operation range of $< 1000\frac{\mu L}{s}$, where laminar flow conditions can still be assumed.

5 Conclusions

This work describes the derivation of an analytical model for the dynamic behavior of a pressure-driven elastomeric membrane-based micropump. The model yields a cubic pressure–displacement law for the non-linear behavior of the membrane as derived from the Young–Laplace equation. This was confirmed by measurement of static deflection and volume transport of the micropump at different pressure levels. The analytical model was further extended to dynamic processes in the microfluidic system by incorporation of Hagen–Poiseuille's law. It can be used both to design microfluidic networks for certain process requirements and to integrate fluidic processes into existing systems.

Two important results are provided by the model which are of particular relevance, e.g. when dealing with biological samples: (i) maximum flow rates that occur during a pump cycle and (ii) the duration of a pump cycle. The model can be used to estimate the influence of system modifications and device related variations, e.g. by the implementation of system dependent pressure actuation courses. In future work, refinements will be added to the model to better account for the boundary conditions when reaching the limit stop.

Appendix

Figs. 10, 11, 12.

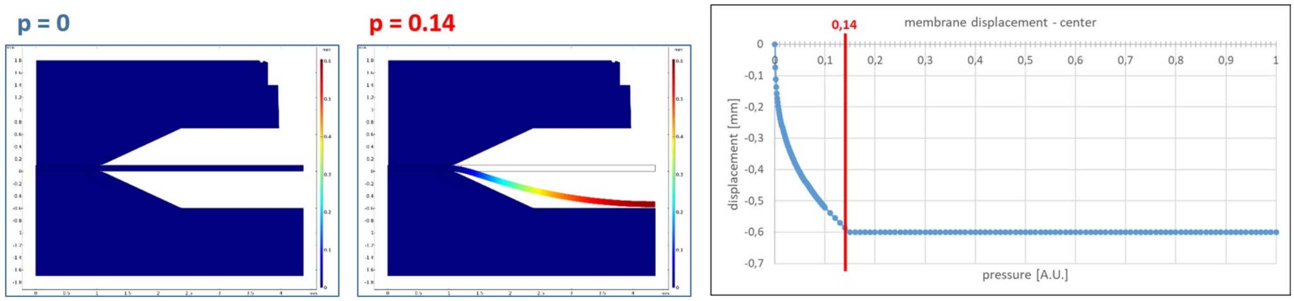

Fig. 10 Numerical simulation to estimate the error resulting from the assumptions for the analytical model. The simulation was set up in COMSOL, computing the displacement of an elastic membrane securely clamped with the form of the investigated pump chamber and displaced through a surface load. As the pump chamber is symmetrical in x and y direction, two symmetry planes were inserted into the model to reduce computing times. The pressure in the COMSOL experiment is given in arbitrary units, as the elastic modulus taken for the membrane in the simulation was estimated and deviates from the actual value. So the membrane displacement as a function of the applied pressure is shown qualitatively but not quantitatively. First, the pressure is determined when the membrane reaches the limit stop which is at 0.6 mm (height of the pump chamber from the zero line of the membrane). The displacement of the center point of the membrane is shown in the graph as a function of pressure. The positions of the membrane at the pressure steps $p = 0$ (zero line of the membrane) and $p = 0.14$ (just before the membrane reaches the maximum displacement) are also displayed

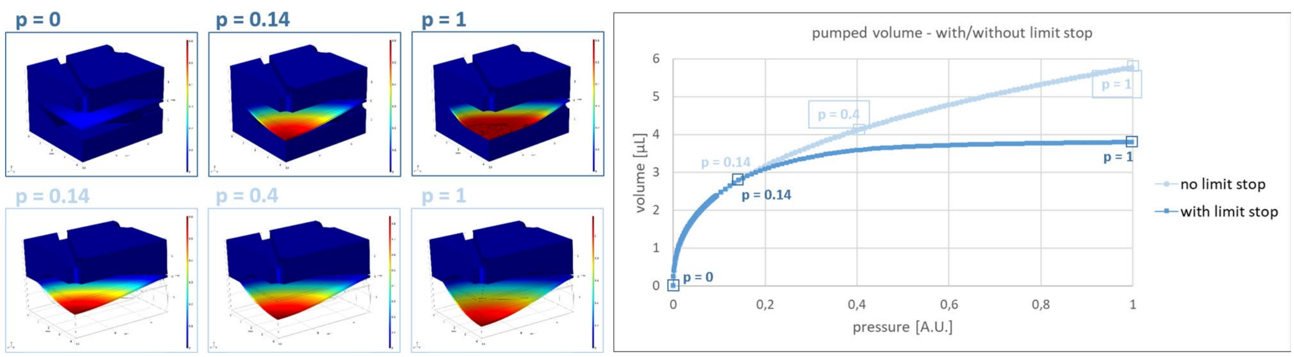

Fig. 11 Two different simulation experiments compared (I) the pressure-dependent displacement of the membrane with a limit stop in the dimensions of the pump chamber (upper row and darker curve) with (II) the pressure-dependent displacement of the membrane without a limit stop (lower row and light curve). The displaced volume was extracted for every simulated pressure step and is shown in the displayed graph. The position of the displaced membrane is shown for the pressure steps $p = 0$, $p = 0.14$, $p = 1$ for simulation (I) and for the pressure steps $p = 0.14$, $p = 0.4$, $p = 1$ for simulation (II). The displaced volume for simulation (I) at $p = 0.14$ is the same as the displaced volume for simulation (II) at $p = 0.14$ which is $V_{\text{pumped}} = 2.785 \mu L$. After $p = 0.14$, when the membrane center reaches the maximum displacement, the two curves start to deviate from each other as the increasing contact area between membrane and pump chamber results in an increasing counterforce and limits the maximal displaceable volume to 3.75 µL (corresponding to $\frac{1}{8}$ of the pump chamber volume for the simulated part of the pump chamber with two symmetry planes and displacement of the membrane from the zero line)

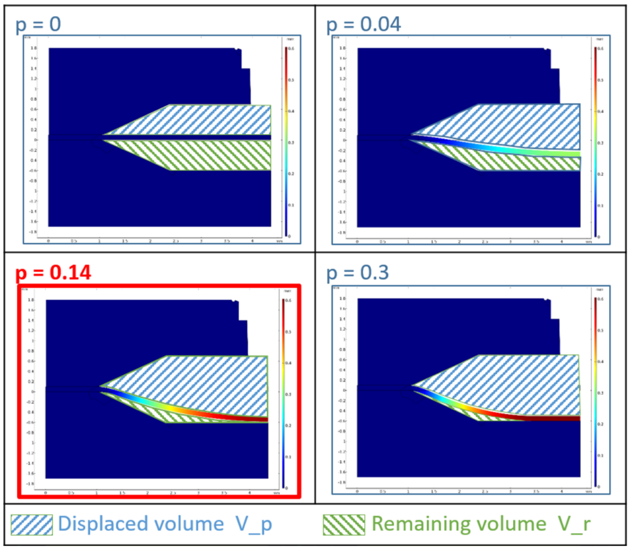

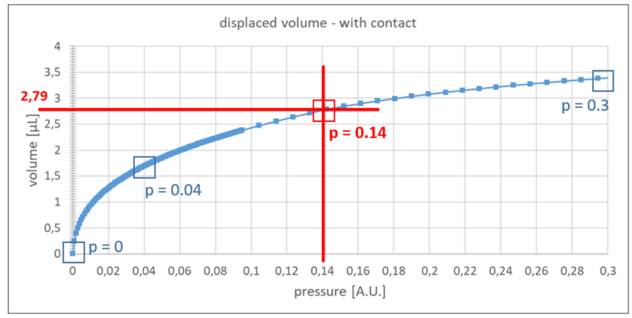

Pressure [A.U]	V_p_model [µL]	V_r _model [µL]	V_p_total [µL]	V_r_total [µL]
0	0.00	3.75	15.0	15.0
0.04	1.70	2.05	21.8	8.2
0.14	2.79	0.95	26.2	3.8
0.30	3.40	0.35	28.6	1.4

Fig. 12 Cross-section of the pump chamber and graphical visualization of the residual volume in the pump chamber at different positions of the displaced TPU-membrane: The pressure-driven displacement of the TPU-membrane was simulated with the same model as described in Fig. 10. For a pressure $p = 0$ the membrane is in its zero position, meaning that 50 % of the pump chamber volume is already pumped out, if the membrane started from its maximum position, being displaced by negative pressure. The membrane is being displaced through applied overpressure, while its center reaches the half of the maximum displacement position from the zero line at $p = 0.04$ and its maximum displacement position at $p = 0.14$. From here the rest of the membrane area is displaced further until every point reaches its maximum displacement position, which would be when the membrane is fully clinging to the pump chamber. The pumped fluid volume as well as the fluid volume that is still in the pump chamber is displayed in the table at $p = 0$, $p = 0.04$, $p = 0.14$ and $p = 0.3$. As the model contains two symmetry planes and the displaced volume is computed from the zero line of the membrane, the total pumped and remaining volume in a pump chamber is shown in the right columns of the table. The row containing the volumes at the contact point of the membrane center with the pump chamber at $p = 0.14$ is highlighted with a box

Acknowledgements The authors are grateful to Juergen Willing for performing the standardized tensile test measurements. The authors thank Roland Zengerle for the discussions on derivation of the model and Bernd Scheufele for proofreading the manuscript.

References

Akers A, Gassman M, Smith R (2006) Hydraulic power system analysis. CRC Press. https://doi.org/10.1201/9781420014587

Au SH, Edd J, Stoddard AE, Wong KHK, Fachin F, Maheswaran S, Haber DA, Stott SL, Kapur R, Toner M (2017) Microfluidic isolation of circulating tumor cell clusters by size and asymmetry. Sci Rep. https://doi.org/10.1038/s41598-017-01150-3

Banejad A, Passandideh-Fard M, Niknam H, Hosseini MJM, Shaegh SAM (2020) Design, fabrication and experimental characterization of whole-thermoplastic microvalves and micropumps having micromilled liquid channels of rectangular and half-elliptical cross-sections. Sensors Actuators A: Phys 301:111713. https://doi.org/10.1016/j.sna.2019.111713

Bardaweel HK, Bardaweel SK (2013) Dynamic simulation of thermopneumatic micropumps for biomedical applications. Microsyst Technol 19(12):2017–2024. https://doi.org/10.1007/s00542-012-1734-3

Berg J, Anderson R, Anaya M, Lahlouh B, Holtz M, Dallas T (2003) A two-stage discrete peristaltic micropump. Sensors and Actuators A: Phys 104(1):6–10. https://doi.org/10.1016/s0924-4247(02)00434-x

Bott H, Leonhardt R, Laermer F, Hoffmann J (2021) Employing fluorescence analysis for real-time determination of the volume displacement of a pneumatically driven diaphragm micropump. J MicromechMicroeng 31(7):075003. https://doi.org/10.1088/1361-6439/ac00c9

Bronstein IN, Semendjajew KA (1991) Taschenbuch der mathematik, 25th edn. Teubner Verlagsgesellschaft, Nauka-Verlag, Leipzig, Moskau, B. G

Brooks DE (1984) The biorheology of tumor cells. Biorheology 21(1–2):85–91. https://doi.org/10.3233/BIR-1984-211-213

Bui G, Wang JH, Lin JL (2017) Optimization of micropump performance utilizing a single membrane with an active check valve. Micromachines 9(1):1. https://doi.org/10.3390/mi9010001

Cheung LSL, Zheng X, Wang L, Baygents JC, Guzman R, Schroeder JA, Heimark RL, Zohar Y (2011) Adhesion dynamics of circulating tumor cells under shear flow in a bio-functionalized microchannel. J Micromech Microeng 21(5):054033. https://doi.org/10.1088/0960-1317/21/5/054033

Chia BT, Liao HH, Yang YJ (2011) A novel thermo-pneumatic peristaltic micropump with low temperature elevation on working fluid. Sensors and Actuators A: Phys 165(1):86–93. https://doi.org/10.1016/j.sna.2010.02.018

Choi S, Lee MG, Park JK (2010) Microfluidic parallel circuit for measurement of hydraulic resistance. Biomicrofluidics 4(3):034110. https://doi.org/10.1063/1.3486609

Dinhof P (2001) Untersuchungen zur beeinflussung der scherempfindlichkeit von CHO-Zellen durch lipoide und cyclodextrine in proteinfreiem Medium. PhD thesis, Universität Hannover. https://doi.org/10.15488/5802

Grover WH, Skelley AM, Liu CN, Lagally ET, Mathies RA (2003) Monolithic membrane valves and diaphragm pumps for practical large-scale integration into glass microfluidic devices. Sensors and Actuators B: Chem 89(3):315–323. https://doi.org/10.1016/s0925-4005(02)00468-9

Guevara-Pantoja PE, Jiménez-Valdés RJ, García-Cordero JL, Caballero-Robledo GA (2018) Pressure-actuated monolithic acrylic microfluidic valves and pumps. Lab Chip 18(4):662–669. https://doi.org/10.1039/c7lc01337j

Henning A (2003) Improved gas flow model for microvalves, vol. 2. pp 1550 – 1553. https://doi.org/10.1109/SENSOR.2003.1217074

Henning A (2006) Comprehensive model for thermopneumatic actuators and microvalves. J Microelectromech Syst 15:1308–1318. https://doi.org/10.1109/JMEMS.2006.879665

Jenke C, Kager S, Richter M, Kutter C (2018) Flow rate influencing effects of micropumps. Sensors Actuators A: Phys 276:335–345. https://doi.org/10.1016/j.sna.2018.04.025

Jeong OC, Park SW, Yang SS (2005) Fabrication and drive test of a peristaltic thermopnumatic PDMS micropump. J Mech Sci Technol 19(2):649–654. https://doi.org/10.1007/bf02916186

Johnson D, Borkholder D (2016) Towards an implantable, low flow micropump that uses no power in the blocked-flow state. Micromachines 7(6):99. https://doi.org/10.3390/mi7060099

Laplace P (1805) Traité de Mécanique Céeste, vol 4. Courcier, Paris, France

Laser DJ, Santiago JG (2004) A review of micropumps. J Micromech Microeng 14(6):R35–R64. https://doi.org/10.1088/0960-1317/14/6/r01

Mazloum J, Shamsi A (2020) 3d design and numerical simulation of a check-valve micropump for lab-on-a-chip applications. J Micro-Bio Robot 16(2):237–248. https://doi.org/10.1007/s12213-020-00139-y

Meng E, Wang XQ, Mak H, Tai YC (2000) A check-valved silicone diaphragm pump. In: Proceedings IEEE Thirteenth Annual International Conference on Micro Electro Mechanical Systems (Cat. No.00CH36308), IEEE. https://doi.org/10.1109/memsys.2000.838491

Mohith S, Karanth PN, Kulkarni S (2019) Recent trends in mechanical micropumps and their applications: a review. Mechatronics 60:34–55. https://doi.org/10.1016/j.mechatronics.2019.04.009

Nguyen NT, Wereley S (2006) Fundamentals and applications of microfluidics, (integrated microsystems), vol 1, 2nd edn. Artech House, Norwood, Massachusetts, USA

Ni J, Li B, Yang J (2012) A pneumatic PDMS micropump with in-plane check valves for disposable microfluidic systems. Microelectron Eng 99:28–32. https://doi.org/10.1016/j.mee.2012.04.002

Oh KW, Lee K, Ahn B, Furlani EP (2012) Design of pressure-driven microfluidic networks using electric circuit analogy. Lab Chip 12:515–545. https://doi.org/10.1039/C2LC20799K

Oosterbroek R, Lammerink T, Berenschot J, Krijnen G, Elwenspoek M, van den Berg A (1999) A micromachined pressure/flow-sensor. Sensors Actuators A: Phys 77(3):167–177. https://doi.org/10.1016/s0924-4247(99)00188-0

Pergal MV, Nestorov J, Tovilović G, Ostojić S, Gođevac D, Vasiljević-Radović D, Djonlagić J (2014) Structure and properties of thermoplastic polyurethanes based on poly(dimethylsiloxane): Assessment of biocompatibility. J Biomed Mater Res 102A:3951–3964. https://doi.org/10.1002/jbm.a.35071

Piccin E, Coltro WKT, da Silva JAF, Neto SC, Mazo LH, Carrilho E (2007) Polyurethane from biosource as a new material for fabrication of microfluidic devices by rapid prototyping. J Chromatogr A 1173(1–2):151–158. https://doi.org/10.1016/j.chroma.2007.09.081

Podbiel D, Boecking L, Bott H, Kassel J, Czurratis D, Laermer F, Zengerle R, Hoffmann J (2020) From CAD to microfluidic chip within one day: rapid prototyping of lab-on-chip cartridges using generic polymer parts. J Micromech Microeng. https://doi.org/10.1088/1361-6439/aba5dd

Poiseuille JLM (1846) Recherches expérimentales sur le mouvement des liquides dans les tubes de très petits diamètres. Mémoires présentés par divers savants à l'Académie royale des sciences de l'Institut de France, Paris, IX:433–544

Pourmand A, Shaegh SAM, Ghavifekr HB, Aghdam EN, Dokmeci MR, Khademhosseini A, Zhang YS (2018) Fabrication of whole-thermoplastic normally closed microvalve, micro check valve, and micropump. Sensors Actuators B: Chem 262:625–636. https://doi.org/10.1016/j.snb.2017.12.132

Richter M, Linnemann R, Woias P (1998) Robust design of gas and liquid micropumps. Sensors Actuators A: Phys 68(1–3):480–486. https://doi.org/10.1016/s0924-4247(98)00053-3

Rupp J, Schmidt M, Muench S, Cavalar M, Steller U, Steigert J, Stumber M, Dorrer C, Rothacher P, Zengerle R, Daub M (2012) Rapid microarray processing using a disposable hybridization chamber with an integrated micropump. Lab Chip 12:1384. https://doi.org/10.1039/C2LC21110F

Salmanzadeh A, Sano MB, Shafiee H, Stremler MA, Davalos RV(2012) Isolation of rare cancer cells from blood cells using dielectrophoresis. In: 2012 Annual International Conference of the IEEE Engineering in Medicine and Biology Society. IEEE. https://doi.org/10.1109/embc.2012.6346000

Schwarz I, Zehnle S, Hutzenlaub T, Zengerle R, Paust N (2016) System-level network simulation for robust centrifugal-microfluidic lab-on-a-chip systems. Lab Chip 16:1873. https://doi.org/10.1039/C5LC01525A

Shaegh SAM, Wang Z, Ng SH, Wu R, Nguyen HT, Chan LCZ, Toh AGG, Wang Z (2015) Plug-and-play microvalve and micropump for rapid integration with microfluidic chips. Microfluid Nanofluidics 19(3):557–564. https://doi.org/10.1007/s10404-015-1582-4

Shaegh SAM, Pourmand A, Nabavinia M, Avci H, Tamayol A, Mostafalu P, Ghavifekr HB, Aghdam EN, Dokmeci MR, Khademhosseini A, Zhang YS (2018) Rapid prototyping of whole-thermoplastic microfluidics with built-in microvalves using laser ablation and thermal fusion bonding. Sensors Actuators B: Chem 255:100–109. https://doi.org/10.1016/j.snb.2017.07.138

Sim WY, Yoon HJ, Jeong OC, Yang SS (2003) A phase-change type micropump with aluminum flap valves. J Micromech Microeng 13(2):286–294. https://doi.org/10.1088/0960-1317/13/2/317

Smits JG (1990) Piezoelectric micropump with three valves working peristaltically. Sensors Actuators A: Phys 21(1–3):203–206. https://doi.org/10.1016/0924-4247(90)85039-7

Sprague I, Kay JL, Bragd MS, Battrell CF (2020) Low elasticity films for microfluidic use. US Patent App. 16/679,076

Tsukinovsky D, Zaretsky E, Rutkevich I (1997) Material behavior in plane polyurethane-polyurethane impact with velocities from 10 to 400 m/sec. J Phys IV Colloq. https://doi.org/10.1051/jp4:1997359

Tuantranont A, Mamanee W, Lomas T, Porntheerapat N, Afzulpurkar NV, Wisitsoraat A (2007) A three-stage thermopneumatic peristaltic micropump for PDMS-based micro/nanofluidic systems. In: 2007 7th IEEE Conference on Nanotechnology (IEEE NANO), IEEE. https://doi.org/10.1109/nano.2007.4601399

Unger MA, Chou HP, Thorsen T, Scherer A, Quake SR (2000) Monolithic microfabricated valves and pumps by multilayer soft lithography. Science 288(5463):113–116. https://doi.org/10.1126/science.288.5463.113

van Lintel HTG, van De Pol FCM, Bouwstra S (1988) A piezoelectric micropump based on micromachining of silicon. Sensors Actuators 15(2):153–167. https://doi.org/10.1016/0250-6874(88)87005-7

Woias P (2005) Micropumps—past, progress and future prospects. Sensors Actuators B: Chem 105(1):28–38. https://doi.org/10.1016/s0925-4005(04)00108-x

Wu WI, Sask KN, Brash JL, Selvaganapathy PR (2012) Polyurethane-based microfluidic devices for blood contacting applications. Lab Chip 12(5):960. https://doi.org/10.1039/c2lc21075d

Wu CH, Chen CW, Kuo LS, Chen PH (2014) A novel approach to measure the hydraulic capacitance of a microfluidic membrane pump. Adv Mater Sci Eng 2014:1–8. https://doi.org/10.1155/2014/198620

Yang YJ, Liao HH (2009) Development and characterization of thermopneumatic peristaltic micropumps. J Micromech Microeng. https://doi.org/10.1088/0960-1317/19/2/025003

Yoon H, Sim WY, Yang S (2001) The fabrication and test of a phase-change micropump. American Society of Mechanical Engineers. Micro-Electromech Syst Div Publ (MEMS) 3:479–484

Yoon SH, Reyes-Ortiz V, Kim KH, Seo YH, Mofrad MRK (2010) Analysis of circular PDMS microballoons with ultralarge deflection for MEMS design. J Microelectromech Syst 19(4):854–864. https://doi.org/10.1109/jmems.2010.2049984

Young WC, Budynas RG (2002) Roark's formulas for stress and strain, 7th edn. McGraw-Hill, New York

Young T (1805) An essay on the cohesion of fluids. Philos Trans Royal Soc London III 95:65–87. https://doi.org/10.1098/rstl.1805.0005

Zengerle R, Richter M (1994) Simulation of microfluid systems. J Micromech Microeng 4(4):192–204. https://doi.org/10.1088/0960-1317/4/4/004